Self-Learning Perfect Optical Chirality via a Deep Neural Network

Yu Li,[1,2,†] Youjun Xu,[3,†] Meiling Jiang,[1,2,†] Bowen Li,[1,2] Tianyang Han,[1,2] Cheng Chi,[1,2] Feng Lin,[1] Bo Shen,[1,2] Xing Zhu,[1] Luhua Lai,[3] and Zheyu Fang[1,2,*]

[1]*School of Physics, State Key Lab for Mesoscopic Physics, Academy for Advanced Interdisciplinary Studies, Nano-optoelectronics Frontier Center of Ministry of Education, Peking University, Beijing 100871, China*

[2]*Collaborative Innovation Center of Quantum Matter, Beijing 100871, China*

[3]*BNLMS, State Key Laboratory for Structural Chemistry of Unstable & Stable Species, College of Chemistry and Molecular Engineering, Peking University, Beijing 100871, Peoples' Republic of China*

(Received 21 June 2019; published 19 November 2019)

Optical chirality occurs when materials interact differently with light in a specific circular polarization state. Chiroptical phenomena inspire wide interdisciplinary investigations, which require advanced designs to reach strong chirality for practical applications. The development of artificial intelligence provides a new vision for the manipulation of light-matter interaction beyond the theoretical interpretation. Here, we report a self-consistent framework named the Bayesian optimization and convolutional neural network that combines Bayesian optimization and deep convolutional neural network algorithms to calculate and optimize optical properties of metallic nanostructures. Both electric-field distributions at the near field and reflection spectra at the far field are calculated and self-learned to suggest better structure designs and provide possible explanations for the origin of the optimized properties, which enables wide applications for future nanostructure analysis and design.

DOI: 10.1103/PhysRevLett.123.213902

Chirality refers to a certain handedness in geometry with the structure mirror image that cannot coincide with itself [1–3]. Although optical chirality widely exists in nature, the chiroptical interaction is weak because of the mismatch between the size of natural materials and the visible wavelength. With the development of advanced nanofabrication techniques, extraordinary structure designs have been realized to achieve strong optical chirality, such as planar spirals [4], antisymmetric bricks [5], gammadions [6,7], and three dimensional metamolecules [8], etc. Automatic and efficient algorithms to optimize and calculate the optical chirality of those nanostructures becomes more important for applications like sensitive detectors and effective spintronic devices.

Machine learning algorithms provide an alternative view for scientific investigation and have played an important role in multiple research fields, such as high-energy particle detection [9], quantum entanglement simulation [10], semiconductor phase transition [11], and compound material designing [12,13], etc. These algorithms were also adapted remarkably in nanophotonics, like resonant mode analysis [14,15], spectra calculation [16,17], and retrieval designing [18–21]. However, for the traditional parametrization process, all of the structure characters are transformed into feature vectors, where the direct geometric information and boundary condition of the structure are neglected; thus the physics interpretability and adaptability are seriously limited. A full picture of light-matter interaction is still challenging for machine learning algorithms.

In this work, we present a self-consistent framework of BoNet [Bayesian optimization (BO) and convolutional neural network (CNN)] for self-learning optical properties of nanostructures in both near field and far field which correspond to electric-field distributions and reflection spectra, and use the BoNet to design nanostructures with optimized chirality in the reflection spectra. Recent advances of CNNs exhibit significant advantages of describing geometric patterns and extracting complex implicit features from pictures [22,23]. BO, as a derivative-free optimization algorithm, is independent of the continuity or derivability of the objective function [24,25]. By investigating designs of nanostructures as pictures, CNN is directly used to build the mapping relationship between the geometric characters of nanostructure patterns and target properties without solving complex Maxwell's functions, which can significantly increase computation efficiency and achieve considerable accuracy for both spectra and electric-field calculation compared with numerical simulations. With performing BO to recommend a set of optimized inputs based on the current state of CNN model, these optimized inputs are used to reinforce the model. This process is iterated several times until the model converges to an allowable error. Then, the converged model is used to recommend optimized nanostructures. It is demonstrated that BoNet is able to implement this efficient and practical platform for optical properties calculation and manipulation.

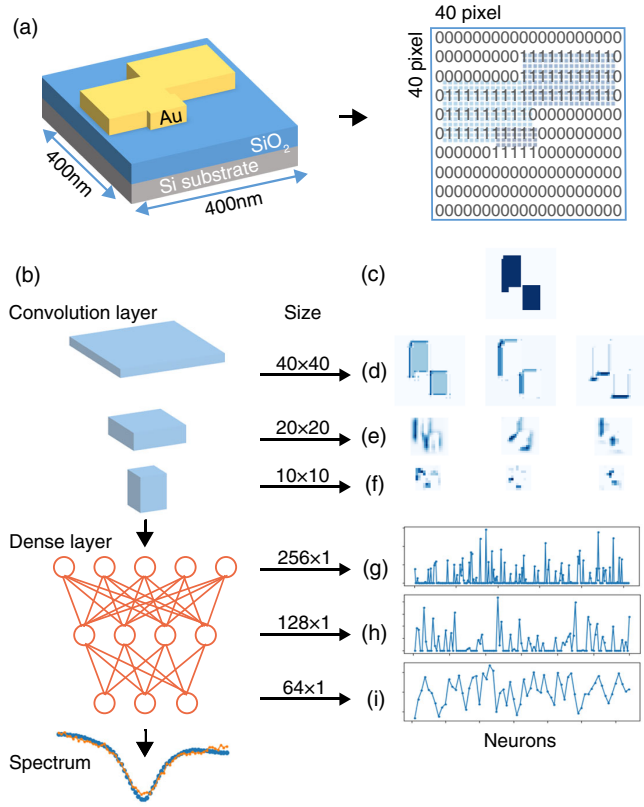

FIG. 1. (a) Nanostructure parametrization. (b) Schematic of BoNet for far-field spectrum calculation. (c) Example structures for feature extraction. (d)–(f) Geometric features extracted from convolution layers with the size of 40×40, 20×20, and 10×10. Boundaries of the pattern are extracted to compute the geometric features that relate with strong electromagnetic resonances. (g)–(i) Vectors extracted from dense layers with the size of 256, 120, and 64 for spectra calculation. Spectrum information is gathered by decreasing number of feature vectors, and finally, the geometric features are transformed into a reflection spectrum.

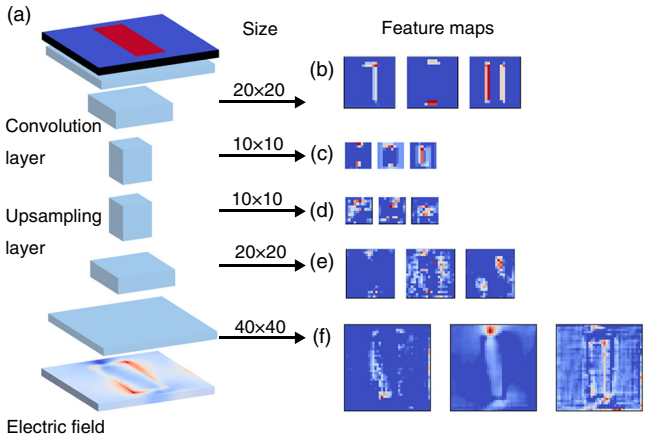

FIG. 2. (a) Schematic of BoNet for near-field calculation. (b) Feature maps extracted from BoNet with the size of 20×20. (c) Feature maps extracted from convolution layers with the size of 10×10. (d) Feature maps extracted from upsampling layers with the size of 10×10. (e) Feature maps extracted from upsampling layers with the size of 20×20. (f) Feature maps extracted from upsampling layers with the size of 40×40. For all feature maps in (b)–(f), x-axis and y-axis locations correspond to the geometric position of the nanostructure, and the normalized color scales (from -1 to 1) show the output values of convolution layers.

The chiral material under investigation is complex thin-film Au nanoantennas composed of discrete Au cubes with fixed dimensions ($10 \times 10 \times 40$ nm^3) positioned on a 40×40 square matrix on the top of a Si/SiO_2 substrate. As shown in Fig. 1(a), a pattern composed of three bricks is represented by a matrix where the area with Au cube (including the overlapping part) is encoded as 1 and the empty area is encoded as 0. Under normal incidence of circularly polarized light, the reflection spectra and electric-field distributions of the complex nanoantennas are calculated by solving Maxwell's equations with boundary conditions, which can be simulated by the finite difference time-domain (FDTD) method. The goal of our approach is utilizing BoNet to predict both reflection spectra and electric-field distributions by training with FDTD numerical simulated data instead of solving Maxwell's equations and automatically generate new structures with optimized spectra.

BoNet is first functionalized to bridge the relation between the structure geometry and its optical response. This network architecture includes two kinds of network layers, convolution layers, and dense layers. Convolution layers extract structure geometric features that are related to optical properties, as shown in Figs. 1(b) and 1(c). On the other side, dense layers are used to map these features to the response of the reflection spectra.

Figure 1(d) exhibits geometric features extracted from the first block of convolution layers. These extracted features with area information contain boundaries of the pattern, which meets the fact that electromagnetic mode resonances depend on the structure boundary conditions. In the second convolution block, the features have less geometric characters but show more characters as electric-field distributions [Fig. 1(e)]. Shown as Fig. 1(f), a few hot spots with a large value in the feature maps are reserved in the last convolution block, and are flattened into dense layers. After complicated calculations in dense layers, the intermediate layers exhibit few activated neurons in the size of 256 and 128 [Figs. 1(g) and 1(h)]. As the dimension reduces to 64, the spectral information is gathered, and more neurons with nonzero weights are utilized for the spectrum calculation [Fig. 1(i)].

Upsampling layers perform three inverse convolution operations, which are connected with convolution layers for the calculation of near-field distribution [Fig. 2(a)]. Feature maps from intermediate layers are shown in Figs. 2(b)–2(f). Figure 2(b) shows that accurate geometric information such as lines and angles is collected from the

first convolution layer. The smaller feature maps in Figs. 2(c) and 2(d) are used to design complicated characters as electromagnetic mode distributions. In Fig. 2(e), characteristic electromagnetic modes of the structure can be concluded in the 20×20 layer, where the location of hot spots can be clearly pointed out. For the last convolution layer, as shown in Fig. 2(f), more detailed characters can be reconstructed and accurately calculated for the electric-field distribution.

To estimate the performance of BoNet, we randomly generate 10 000 samples and run FDTD simulations to provide corresponding optical properties including reflection and electric-field distribution. Considering the symmetries of boundary condition, the samples are augmented 8 times (see Supplemental Material [26], S1) and divided into 3 parts: 80% for training, 10% for validation, and 10% for testing. The loss function is defined as the mean square error (MSE) between the outputs of FDTD simulation and BoNet. The optimization algorithm Adam (adaptive moment estimation with the learning rate of 0.001) is used to minimize the loss function [27]. After training 100 epochs, the well-built models can directly predict both the reflection spectra and electric-field distribution. The MSE for electric-field prediction is 0.048 for training data and 0.068 for validation and testing data, which is sufficient to predict electromagnetic mode distribution near the metallic structures and provide knowledge for nanoantenna design. For reflection spectra, training loss is 1.30×10^{-4}, validation loss is 3.52×10^{-4}, and testing loss is 3.74×10^{-4}. Compared with traditional numerical simulations, BoNet directly predicts the character response by matrix transformation without solving the Maxwell equations, providing a rapid approach for calculating target properties (see Supplemental Material [26], S2).

Then, we iteratively use BO to enhance the CNN model. First, BO is performed to optimize optical properties (Y), as the objective function of CNN, which means BO can recommend new parameters (X) with improved Y. However, in our system, CNN is originally trained by random examples with a small Y value; thus samples with a large Y value are hard for CNN prediction (see Supplemental Material [26], S3). Therefore, the second strategy is utilizing BO to improve the prediction accuracy for samples with a large Y value. Based on the next generation of X, the corresponding Y is calculated by both CNN (Y_{CNN}) and FDTD (Y_{FDTD}). By validating the error between Y_{CNN} and Y_{FDTD}, the sensitivity of the system can be evaluated. For a system with a strong sensitivity (large error between Y_{CNN} and Y_{FDTD}), samples with improved Y are added into the training dataset and used to retrain CNN to improve the prediction accuracy (see Supplemental Material [26], S4, S5). During the loop of optimization, more FDTD validation improves calculation accuracy but slows down the speed. In the mission of designing nanostructure with optimized optical chirality, 20% of samples recommended by BO are evaluated by FDTD then used to extend the training dataset for improving the CNN.

Optical chirality is widely applied in biosensors, detectors, and tunable optoelectronic devices [28–30]. Realizing strong optical chirality is important for high signal-noise-ratio device applications [31]. Here, we attempt to maximize the circular dichroism (CD) of designed structure by using the BoNet framework. To simplify the optimization process, the target wavelength is first fixed at 650 nm. Intermediate structures are plotted to illustrate the self-learning process of this CD enhancement, as shown in Fig. 3(a).

Different colors are used to represent their comparative CD intensities. Brown structures are best designs for each generation, and their corresponding CD intensities are extracted as Fig. 3(b), where we can see the initial intensity is rather weak for the randomly generated structures as the first generation. For the second generation, the BO sampling strategy is an exploration operation to increase the variety of designs, since most of the structures are still unknown and contribute to uncertainty in the parameter space. The calculated CD is steadily enhanced for latter generations with the BoNet self-learning. As optimization continues, structures in the fourth and fifth generations present more similarity. And BO sampling strategy changes to exploitation, which means the fine-tuning of structure parameters. After about five generations, the CD maximization at the target wavelength of 650 nm is achieved and an almost perfect optical chirality is realized.

A statistical description of the BoNet self-learning process in each generation is also provided and shown in Fig. 3(c). The CD distribution is defined as the dependency between the CD intensity and the number of corresponding structures. The shape of CD distribution gradually changes from fusiform to dumbbell with the calculated generations, which means the accuracy of BoNet calculation is improved, and more designed structures can present strong CD in the latter generations. Because neural network strongly depends on the training data, structure designs in early generations are automatically collected and used to retrain the CNN neurons. This recycle process extremely expands the knowledge region of CNN, and achieves an effective improvement for both target properties optimization and self-learning accuracy. More structures with strong CD are generated by BoNet to accelerate the parameter searching for the robust enhancement, which finally approaches the perfect optical chirality.

BoNet is also adaptive for multiple parameters calculation. For example, the CD maximization can be also realized when we changed the target wavelength from 650 to 800 nm, as shown in Fig. 3(d), where the CD increases steadily, and the perfect optical chirality can be achieved at different calculated generations for various target wavelengths.

To validate the practical application of BoNet, the designed structures were fabricated by using E-beam lithography and characterized by reflection microspectroscopy (see Supplemental Material [26], S6). The measured CD

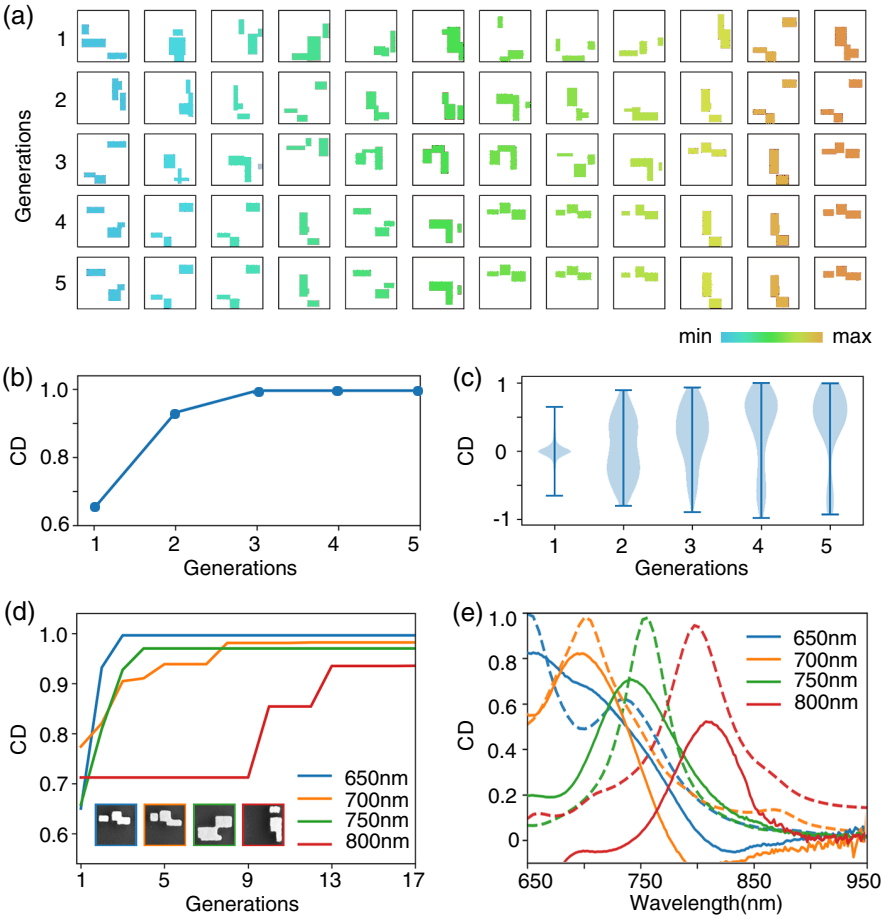

FIG. 3. Far-field CD optimization. (a) Intermediate structures designed by BoNet with different far-field CD intensities in each generation. (b) CD intensities of best designs for each generation. (c) Statistical description of the BoNet self-learning process in each generation. (d) CD optimization at various target wavelengths. Insets: SEM images of structures with strongest CD at wavelengths of 650, 700, 750, and 800 nm. (e) BoNet calculated and corresponding experimental far-field CD spectra at target wavelength of 650, 700, 750, and 800 nm.

spectra are plotted in Fig. 3(e), where the enhanced chirality at each target wavelength (solid line) agrees with the BoNet expectation (dashed line). The experimental acquired CD is about 0.82 at target wavelength of 650 nm, the discrepancy between the measured result and calculation may come from the tolerance of sample fabrication and measurements. As the target wavelength changed to 800 nm, the measured CD decreases to ~0.5, which is resulted from the decreasing of incident light intensity and the attenuation of the polarizer extinction coefficient at the near-infrared regime.

In order to explore the origin of this perfect optical chirality, five representative structures during the BoNet self-learning process were fabricated by using *E*-beam lithography and following the lift-off process, shown as the SEM images in Fig. 4(a). The measured far-field CD spectra are plotted in Fig. 4(b), where we can see the first generated single brick structure exhibits an achiral background, which is used as the CNN training data for the next structure design. With the initial BoNet self-learning, the second generated structure gives a rather flat spectrum with a weak CD intensity. However, the superiority of BoNet self-learning ability that merges both merits of BO and CNN rapidly makes the third promoted structure to present strong circular dichroism that is larger than 0.6 with its resonant wavelength close to 650 nm. Further optimization makes the CD increase to 0.7 at exactly the target wavelength of 650 nm for the fourth generated structure. The last promoted structure with an almost perfect optical chirality at 650 nm is finally achieved, and with a strong CD in a wide spectral range.

As we discussed before, BoNet can simultaneously calculate the near-field distribution for the generated structure, which provides a detailed physics explanation for the origin of obtained strong CD. Given electromagnetic distributions in the near field, the reflection spectra in the far field can be calculated (see Supplemental Material [26], S2). For the CNN algorithm, the network for far- and near-field calculation shares convolutional layers for the

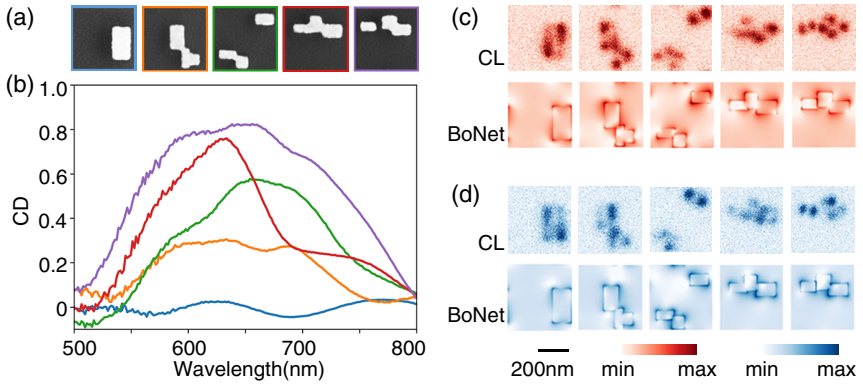

FIG. 4. Analysis of perfect optical chirality. (a) SEM images of structures in the optimization process at target wavelength of 650 nm. (b) Experimentally acquired CD spectra of five structures in (a). (c) The LCP component of CL mapping for the structures in (a) and corresponding BoNet calculated electric-field distributions. (d) The RCP component of CL mapping for the structures in (a) and corresponding BoNet calculated electric-field distributions.

electromagnetic character extraction. Once CNN is well trained, the relationship between the electric-field distribution and structure geometry can be fully established, which enables further calculation of far-field spectra by the dense layer in the CNN algorithm.

In order to study the detail of electromagnetic mode resonance, the cathodoluminescence (CL) spectroscopy with ultrahigh resolution was used to measure the optical near-field distribution of these nanostructures (see Supplemental Material [26], S6). Metallic nanoparticles are usually considered as optical antennas, and their near-field radiations have been confirmed and can be described by the CL mapping [32–35]. All of the fabricated nanostructures were scanned by a focused electron beam, and corresponding excited CL emissions were recorded to realize an intensity mapping. A set of bandpass filter and circular polarizer were used to extract either left-handed circularly polarized (LCP) or right-handed circularly polarized (RCP) CL component, as shown on the top of Figs. 4(c) and 4(d), which has excellent agreement with the electric-field distribution calculated by the BoNet and plotted at the bottom of Figs. 4(c) and 4(d).

From these CL mapping images, all of the electric-field hot spots located at corners of the nanostructure can be clearly distinguished. For the first single brick structure, because of the mirror symmetry, the energy flow from near-field radiation into the far field is identical for the far-field scattering, which leads to an achiral background. However, when the hot spot distribution cannot overlap with itself under the rotation or mirror operations, the radiation of structure is diverse and results in a strong far-field CD. For example, the second generated structure shows five hot spots under LCP excitation, but only two hot spots exist when the excitation changed to RCP. For structures in latter generation, a stronger difference of the hot spot distribution can be found under LCP or RCP excitation, and finally the structure with a perfect optical chirality is generated, where most of the energy is absorbed under RCP excitation, and it results in a nearly 100% CD in the far-field spectra.

In conclusion, an intelligent self-learning platform named BoNet was proposed for the nanophotonic properties optimization. The distinctive self-consistent framework enables BoNet to self-learn the obtained properties and shows the ability for global optimization. In this work, BoNet was used to investigate both optical farfields and near fields for the perfect optical chirality. A theoretical CD maximum was achieved with a corresponding experimental result of 82% obtained in the far field. The CL spectroscopy was applied to analyze the origin of this strong optical chirality, where the asymmetric distribution of the near-field hot spots under LCP or RCP excitation results in the strong far-field CD.

Furthermore, with more controllable parameters taken into consideration, the proposed BoNet platform can be used for any other nanophotonic structures with their specific applications. This probabilistic distribution based self-learning platform provides new insight to analyze the design structure and its corresponding optical properties directly from the numerical data without solving Maxwell's equations. This study can also inspire more applications of neural networks and machine learning algorithms for the analysis of nanostructures, and improve the workflow of future nanophotonics studies.

This work is supported by the National Key Research and Development Program of China (Grant No. 2017YFA0206000), National Basic Research Program of China (Grants No. 2015CB932403, No. 2017YFA0205700, and No. 2019YFA0210203), National Science Foundation of China (Grants No. 11674012, No. 61521004, No. 21790364, No. 61422501, and No. 11374023), Beijing Natural Science Foundation (Grants No. Z180011 and No. L140007), and Foundation for the Author of National Excellent Doctoral Dissertation of China (Grant No. 201420), National Program for

Support of Top-notch Young Professionals (Grant No. W02070003).

*Corresponding author.
zhyfang@pku.edu.cn
†These authors contributed equally to this work.

[1] J. B. Pendry, Science **306**, 1353 (2004).
[2] Y. Tang and A. E. Cohen, Phys. Rev. Lett. **104**, 163901 (2010).
[3] A. Drezet, C. Genet, J.-Y. Laluet, and T. W. Ebbesen, Opt. Express **16**, 12559 (2008).
[4] Y. Gorodetski, A. Drezet, C. Genet, and T. W. Ebbesen, Phys. Rev. Lett. **110**, 203906 (2013).
[5] C. Wu, N. Arju, G. Kelp, J. A. Fan, J. Dominguez, E. Gonzales, E. Tutuc, I. Brener, and G. Shvets, Nat. Commun. **5**, 3892 (2014).
[6] A. Papakostas, A. Potts, D. M. Bagnall, S. L. Prosvirnin, H. J. Coles, and N. I. Zheludev, Phys. Rev. Lett. **90**, 107404 (2003).
[7] E. Hendry, T. Carpy, J. Johnston, M. Popland, R. V. Mikhaylovskiy, A. J. Lapthorn, S. M. Kelly, L. D. Barron, N. Gadegaard, and M. Kadodwala, Nat. Nanotechnol. **5**, 783 (2010).
[8] A. Kuzyk, R. Schreiber, H. Zhang, A. O. Govorov, T. Liedl, and N. Liu, Nat. Mater. **13**, 862 (2014).
[9] P. Baldi, P. Sadowski, and D. Whiteson, Nat. Commun. **5**, 4308 (2014).
[10] G. Torlai, G. Mazzola, J. Carrasquilla, M. Troyer, R. Melko, and G. Carleo, Nat. Phys. **14**, 447 (2018).
[11] E. P. L. van Nieuwenburg, Y.-H. Liu, and S. D. Huber, Nat. Phys. **13**, 435 (2017).
[12] Q. Zhou, P. Tang, S. Liu, J. Pan, Q. Yan, and S. C. Zhang, Proc. Natl. Acad. Sci. U.S.A. **115**, E6411 (2018).
[13] T. Xie and J. C. Grossman, Phys. Rev. Lett. **120**, 145301 (2018).
[14] C. Barth and C. Becker, Commun. Phys. **1**, 58 (2018).
[15] D. Zibar, H. Wymeersch, and I. Lyubomirsky, Nat. Photonics **11**, 749 (2017).
[16] W. Ma, F. Cheng, and Y. Liu, ACS Nano **12**, 6326 (2018).
[17] J. Peurifoy, Y. Shen, L. Jing, Y. Yang, F. Cano-Renteria, B. G. DeLacy, J. D. Joannopoulos, M. Tegmark, and M. Soljačić, Sci. Adv. **4**, eaar4206 (2018).
[18] S. Molesky, Z. Lin, A. Y. Piggott, W. Jin, J. Vucković, and A. W. Rodriguez, Nat. Photonics **12**, 659 (2018).
[19] I. Malkiel, M. Mrejen, A. Nagler, U. Arieli, L. Wolf, and H. Suchowski, Light Sci. Appl. **7**, 60 (2018).
[20] D. Liu, Y. Tan, E. Khoram, and Z. Yu, ACS Photonics **5**, 1365 (2018).
[21] Z. Liu, D. Zhu, S. P. Rodrigues, K. T. Lee, and W. Cai, Nano Lett. **18**, 6570 (2018).
[22] A. Krizhevsky, I. Sutskever, and G. E. Hinton, Commun. ACM **60**, 84 (2017).
[23] J. Long, E. Shelhamer, and T. Darrell, IEEE Trans. Pattern Anal. Mach. Intell. **39**, 640 (2016).
[24] Z. Ghahramani, Nature (London) **521**, 452 (2015).
[25] S. Ju, T. Shiga, L. Feng, Z. Hou, K. Tsuda, and J. Shiomi, Phys. Rev. X **7**, 021024 (2017).
[26] See Supplemental Material at http://link.aps.org/supplemental/10.1103/PhysRevLett.123.213902 for data preparation, calculation advantages of CNN, mathematical derivation of BO, as well as experimental methods for reflection spectra and CL.
[27] D. Kingma and J. Ba, arXiv:1412.6980.
[28] W. Ma, H. Kuang, L. Xu, L. Ding, C. Xu, L. Wang, and N. A. Kotov, Nat. Commun. **4**, 2689 (2013).
[29] M. Khorasaninejad and K. B. Crozier, Nat. Commun. **5**, 5386 (2014).
[30] S. Ostovar pour, L. Rocks, K. Faulds, D. Graham, V. Parchansky, P. Bour, and E. W. Blanch, Nat. Chem. **7**, 591 (2015).
[31] T. Yiqiao and A. E. Cohen, Science **332**, 333 (2011).
[32] S. Zu, T. Han, M. Jiang, F. Lin, X. Zhu, and Z. Fang, ACS Nano **12**, 3908 (2018).
[33] S. Zu, T. Han, M. Jiang, Z. Liu, Q. Jiang, F. Lin, X. Zhu, and Z. Fang, Nano Lett. **19**, 775 (2019).
[34] F. J. García de Abajo, Rev. Mod. Phys. **82**, 209 (2010).
[35] T. Han, S. Zu, Z. Li, M. Jiang, X. Zhu, and Z. Fang, Nano Lett. **18**, 567 (2018).